Multi-shelled CeO2 hollow microspheres as superior photocatalysts for water oxidation

Author

Qi, Jian, Zhao, Kun, Li, Guodong, Gao, Yan, Zhao, Huijun, Yu, Ranbo, Tang, Zhiyong

Published

Journal Title

Version

DOI

Copyright Statement

Downloaded from

Griffith Research Online

Nanoscale

Dynamic Article Links ▶

COMMUNICATION

Multi-Shelled CeO₂ Hollow Microspheres as Superior Photocatalysts for Water Oxidation†

Jian Qi,[‡a] Kun Zhao,[‡ab] Guodong Li,[‡a] Yan Gao,[a] Huijun Zhao,[c] Ranbo Yu[*b] and Zhiyong Tang[*a]

A general self-templating method is introduced to construct triple-shelled CeO₂ hollow microspheres, which are composed of tiny CeO₂ nanoparticles. When the triple-shelled CeO₂ hollow microspheres are used as photocatalysts for direct
10 **water oxidation with AgNO₃ as the electron scavenger, the excellent activity and the enhanced stability for O₂ evolution are achieved in contrast with commercial CeO₂ nanoparticles, single-shelled CeO₂ hollow microspheres and double-shelled CeO₂ hollow microspheres. Such an outstanding performace**
15 **is attributed to the unique properties of the triple-shelled CeO₂ hollow microspheres including more efficient multiple reflections of the incident light by inner shells, the larger surface area and more active sites for improving separation of electron and hole pairs, and the more curved surfaces**
20 **unfavorable for deposition of *in-situ* generated Ag nanoparticle.**

Solar water splitting directly to hydrogen and oxygen has become one of the most desirable ways for harvesting and conversion of solar energy into chemical energy, since Fujishima and Honda 25 first discovered photocatalytic conversion of water into hydrogen and oxygen using TiO₂ in 1972.[1] Because the overall water splitting is a typical "uphill reaction",[2] the photocatalytic performance of a semiconductor for water splitting into hydrogen and oxygen is usually evaluated independently in the presence of 30 sacrificial electron donors (*e.g.*, methanol[3]) or electron acceptors (*e.g.*, silver nitrate[4]). Among two half reactions, water reduction reaction has been intensively investigated and a number of efficient photocatalysts including oxides,[5] nitrides,[6] oxynitrides,[7] and sulfides[8] have been developed. As comparison, only few 35 active photocatalysts are obtained for direct water oxidation. The great challenge lies in the fact that oxidation of water simultaneously requires four hole equivalents to produce one oxygen molecule, which is conceptually more difficult than reduction of water to hydrogen requiring two electrons.[9] To 40 obtain the photocatalysts for water oxidation, many efforts have devoted to preparation of nanosized solid particles and composite oxides, such as WO₃,[10] CeO₂,[11] Fe₂O₃,[12] BiVO₄[13] and WO₃/BiVO₄.[14] Though these catalysts exhibit the improved performance for photocatalytic water oxidation,[15] the low 45 efficiency is still remained, which should originate from the following aspects: (1) Low incident light absorption,[16] (2) fast recombination of electron and hole pairs,[17] and (3) low

photocatalytic stability.[18] Previous studies have demonstrated that transition metal oxides of hollow micro-/nano-structure including 50 TiO₂,[19] ZnO,[20] Cu₂O,[21] Co₃O₄,[22] SnO₂,[23] and Fe₃O₄[24] are the promising photocatalysts in organic pollutant degradation and dye-sensitized solar cells, owing to their low density, large surface area and high light-harvesting efficiency.[25] Unexpectedly, to use the hollow micro-/nano-structures as the photocatalysts for 55 direct water oxidation is very rare.[26] In this work, we suggest introducing the hollow micro-/nano-structures, expecially multi-shelled hollow structures, to replace the popular solid particles for photocatalytic water oxidation.

CeO₂ as one of the most important semiconductor materials 60 possesses the exceptional catalytic oxidation properties due to its abundant oxygen vacancy defects, high oxygen storage capacity and the relatively easy shuttles between III and IV oxidation state,[27] thus encouraging us to explore the water oxidation efficiency by using hollow CeO₂ micro-/nano-structures. Herein, 65 a novel and simple self-templating approach, rather than the conventional soft- or hard-templating methods,[28] is adopted to construct the multi-shelled CeO₂ hollow microspheres (MSCeHSs). The synthetic recipe involves dissolution of CeCl₃ precursors in the mixed aqueous solution containing glucose and 70 urea, followed by hydrothermal and calcination treatments. Scheme 1 illustrates the detailed formation process of the MSCeHSs: Firstly, condensation and polymerization of glucose in aqueous solution under the hydrothermal condition give rise to formation of carbon microspheres. Subsequently, the functional 75 groups inside the carbon microspheres are deprotonated in the alkaline environment from decomposition of urea, which enable adsorption of Ce³⁺ ions through electrostatic attractions. Finally, as-formed carbon microspheres are used as the sacrificial templates to obtain the triple-shelled CeO₂ hollow microspheres 80 (TSCeHSs) via calcination in air. Impressively, when the TSCeHSs are utilized as the photocatalysts for direct water
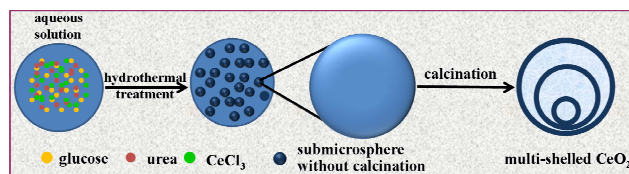
Scheme 1. Schematic diagram for construction of MSCeHSs via
85 hydrothermal and calcination treatments.

Nanoscale Accepted Manuscript

oxidation, they exhibit the excellent activity and the improved stability compared with commercial CeO_2 NPs, single-shelled CeO_2 hollow microspheres (SSCeHSs) and double-shelled CeO_2 hollow microspheres (DSCeHSs).

The morphology and the structure of as-synthesized TSCeHSs products are firstly investigated by different characteriztion techniques (Fig. 1), and several important features may be discerned: (1) Scanning electron microscopy (SEM) image shows that the products are roughly spherical in shape with a rather narrow size distribution of about 1-2 μm (Fig. 1a), and while transmission electron microscopy (TEM) image indicates that these microspheres are exclusively characteristic of triple-shelled hollow structure and sphere-in-sphere morphology (Fig. 1b). (2) Elemental mapping by high angle annular dark field scanning transmission electron microscopy (HAADF-STEM) reveals that elements Ce and O are homogeneously distributed inside the triple-shelled hollow microspheres (Fig. 1c), and individual shell is enriched of Ce and O elements, which are also consistent with the result from STEM-EDS line scans (Fig. 1c). (3) The CeO_2 shell is composed of many small NPs with the diameters of about 5 nm (Fig. 1d), and high-resolution transmission electron microscopy (HRTEM) image further discloses that individual NPs in the shell are highly crystalline with the interplanar spacings of 0.31 nm, 0.27 nm and 0.19 nm, corresponding to the (111), (200) and (220) planes of fluorite-type CeO_2, respectively (Fig. 1e). (4) Powder X-ray diffraction (XRD) pattern confirms that the TSCeHSs are composed of fluorite-type CeO_2 (Fig. 1f).[29] It should be pointed out that the broad peaks assinged to amorphous carbon from condensation and polymerization of glucose are not found in the final products (Fig. 1f), implying that carbon source in the microspheres is removed completely via the calcination treatment in air.
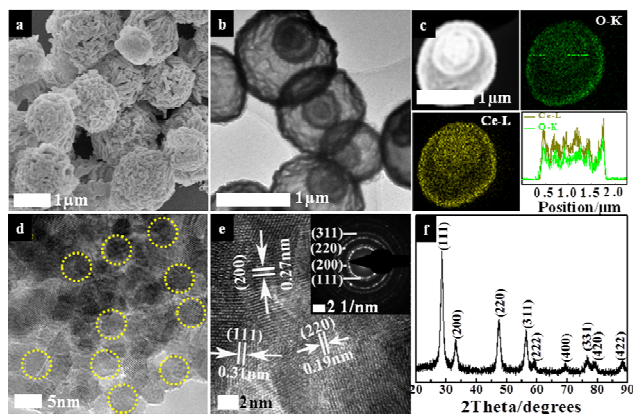
Fig. 1 (a) SEM image of TSCeHSs. (b) TEM image of TSCeHSs. (c) HAADF-STEM mapping image of the microsphere and the corresponding line-scan profiles. (d) and (e) HRTEM images of the microspheres. Inset is SAED image, indicating polycrystalline nature of the CeO_2 shell. (f) XRD pattern of the microsphere.

In order to elucidate the formation process of the TSCeHSs, the intermediate products after hydrothermal process and without calcination treatment, denoted as pre-TSCeHSs, are analyzed (Fig. 2). The products are also roughly spherical in shape, and the sizes are about 4-7 μm in diameter (Fig. 2a), which are considerably larger than those of the TSCeHSs (Fig. 1a-b). Meanwhile, elemental mapping by HAADF-STEM reveals that elements Ce,

C and O are homogeneously distributed in the whole pre-TSCeHSs (Fig. 2b). This observation indicates that adsorption of Ce^{3+} ions is simultaneous with the growth of carbon matrix. Crystal structure survey based on XRD pattern displays a broad peak corresponding to amorphous nature of carbon matrices (starred peak in Fig. 2c), while the characteristic peaks of cerium-based compounds in the pre-TSCeHSs are not distinguished, suggesting that they are presented in the microspheres in the form of amorphous nature. X-ray photoelectron spectroscopy (XPS) measurement of the pre-TSCeHSs further shows two Ce^{3+} 3d peaks at 885.1 eV and 904.0 eV (Fig. 2d),[30] which confirms the hypothesis that Ce^{3+} ions are adsorbed into the carbon matrix of the pre-TSCeHSs during the hydrothermal process. Accordingly, the transformation of Ce^{3+} into Ce^{4+} should occur in the subsequent calcination process, which is evidenced by the XPS study of the final TSCeHS products (Fig. S1).
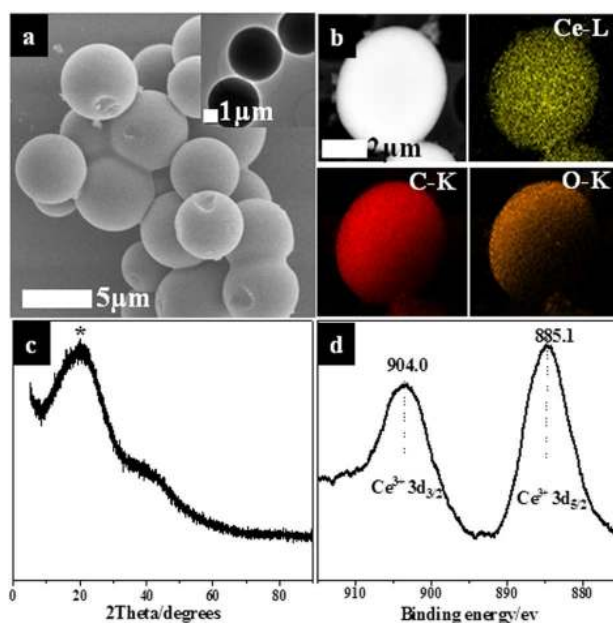
Fig. 2 (a) SEM image and TEM image (inset) of pre-TSCeHSs. (b) HAADF-STEM mapping image of the microsphere. (c) and (d) Corresponding XRD and XPS patterns of (a).

A series of control experiments including variation of glucose, urea, $CeCl_3$, crystallization temperature, crystallization time and calcination temperature were performed to rationalize synthesis of the TSCeHSs as well as to explore the formation mechanism. Fig. S2 shows that the product morphologies are dendritic, solid spherical and triple-shelled hollow spherical structures in sequence with increasing the amount of glucose from zero to a high amount in the mixed solution containing $CeCl_3$ and urea. This result discloses that glucose acts as an important role in determining the morphologies of final products. To further understand transformation of glucose, the functional groups in the pre-TSCeHSs are identified by Fourier transform infrared (FT-IR) spectroscopy. It is seen from Fig. S3 that: (1) The absorption bands at 1695 and 1617 cm^{-1} that are ascribed to C=O and C=C vibrations demonstrate aromatization of glucose.[31] (2) The appearance of the COO^- stretching absorption at 1370 cm^{-1} mainly originates from carbonization of glucose.[32] (3) The bands in the range of 1000-1300 cm^{-1} include the C-OH stretching and

OH bending vibrations, suggestive of existence of the residual hydroxy groups. These FT-IR results indicate that carbonization of glucose offers the carbon source to produce the sacrificial templates with aboundant functional groups. Urea is found to be another important factor to influence the product morphology. In absence of urea, irregular particles are formed. While with increasing the amount of urea the morphologies of the products are triple-shelled hollow spherical and solid spherical in sequence (Fig. S4). Decomposition of urea would release OH^- ions, which promote deprotonation of the functional groups inside carbon microspheres and simultaneous formation of COO^- ions. When more COO^- ions are formed, more Ce^{3+} ions could be adsorbed through electrostatic attraction, leading to transformation from hollow to solid spherical CeO_2. Differently, the added amount of $CeCl_3$ has little effect on the formation of the TSCeHSs under the hydrothermal conditions used (Fig. S5). Moreover, the influences of crystallization temperature, crystallization time and calcination temperature on the final products are also investigated and the results are shown in Fig. S6, S7 and S8. It should be noted that the available products are either solid NPs or TSCeHSs, and no other hollow structures of single shell or double shells are achieved under the experimental conditions used, likely owing to the difficulty in controlling the nucleation and growth rate of cerium-based compounds in the carbon matrices under the hydrothermal conditions (Fig. S9).

The catalytic performance of TSCeHSs was evaluated as the photocatalysts for direct water oxidation. As comparison, the commercial CeO_2 NPs are purchased, and the SSCeHSs and the DSCeHSs samples are synthesized by using different methods (see Electronic Supplementary Information).[33] Before examination of the catalytic performances, the physiochemical properties of the commercial CeO_2 NPs, the SSCeHSs, the DSCeHSs and the TSCeHSs are determined. XRD patterns indicate that all the samples have the similar fluorite-type crystal phase (Fig. 1, S10, S11 and S12). SEM and TEM images show that the commercial CeO_2 NPs have the sheet-like structure and are composed by NPs of about 20-30 nm in diameter (Fig. S10), the SSCeHSs are 300-400 nm in diameter and composed by NPs of about 6-13 nm in diameter (Fig. S11), while the DSCeHSs are about 350-450 nm in diameter and composed by NPs of about 5-8 nm in diameter (Fig. S12). Brunauer-Emmett-Teller (BET) data displays that the specific surface areas are 5.1 m^2 g^{-1} for the commercial CeO_2 NPs, 53.1 m^2 g^{-1} for the SSCeHSs, 55.8 m^2 g^{-1} for the DSCeHSs and 79.5 m^2 g^{-1} for the TSCeHSs, respectviely (Fig. S13 and Table S1). Generally, all the samples possess the same crystalline structures, have comparable sizes except for TSCeHSs (about 2-3 times larger), and are composed of small CeO_2 NPs with the sizes of several to several ten nanometers. The obvious difference in the BET data is easily understood that the hollow microspheres with more shells should have larger surafce areas. Fig. 3 summarizes the O_2 evolution as a function of reaction time over different photocatalysts with $AgNO_3$ as the electron scavenger under the UV light irradiation (250 nm $<$ λ $<$380 nm). It is evident that the catalytic activity of the TSCeHSs is much higher than that of the commercial CeO_2 NPs, the SSCeHSs and the DSCeHSs. The average O_2 evolution rates from water oxidation are 14 μmol g^{-1}_{cat} h^{-1} for the commercial CeO_2 NPs, 30 μmol g^{-1}_{cat} h^{-1} for the SSCeHSs, 46 μmol g^{-1}_{cat} h^{-1} for

the DSCeHSs and 78 μmol g^{-1}_{cat} h^{-1} for the TSCeHSs, respectively. Such a superior performance of the TSCeHSs mainly originates from the following two aspects: (1) The TSCeHSs have three interior cavity compartments, while the commercial CeO_2 NPs, the SSCeHSs and the DSCeHSs have zero, one and two cavities, respectively. Such multi-shelled hollow structure allows for more multiple reflections of the incident light (Fig. S14), resulting in more efficient use of the incident light and the enhanced catalytic activity.[34] The increased reflection capability of the TSCeHSs is also supported by UV-Vis diffuse-reflectance spectrum survey on the four photocatalysts (Fig. S15), indicating that more photogenerated electron and hole pairs could be excited when TSCeHSs are used as photocatalysts under the UV irradiation condition.[35] (2) The individual CeO_2 NPs in TSCeHSs are the smallest among four samples used (Fig. 1, S10-S12), suggesting the distance that photogenerated electrons and holes have to migrate to the active sites on the surface of TSCeHSs is the shortest, leading to a decrease in the recombination probability.[36] Also, the TSCeHSs have larger surface area and more active sites (Table S1), which are favorable for both capture of the conduction band electrons by Ag^+ ions and consumption of the valence band holes consumed by OH^- ions to produce O_2, thus promoting separation of the electron and hole pairs. We also notice that the O_2 evolution during the photocatalytic process is likely to be partially contributed from redox reaction of $AgNO_3$, since $AgNO_3$ itself may be decomposed under the photoirradiation condition to generate O_2. To exclude this effect, the blank experiment of $AgNO_3$ aqueous solution without any other photocatalysts is performed under the same conditions of Fig. 3. When illumination time lasts for 4 h, small amount of precipitate is formed and gas product analysis by on-line gas chromatograph displays that O_2 evolution from $AgNO_3$ decomposition is less than 4% of that with TSCeHSs (Fig. S16), disclosing that the effect of $AgNO_3$ decomposition on O_2 evolution under the photoirradiation condition can be neglected. Furthermore, photocatalytic water oxidation experiment by the TSCeHSs in the absence of Ag^+ ions is also carried out and no O_2 evolution happens, revealing that the electron scavenger used is necessary for O_2 evolution in this system.
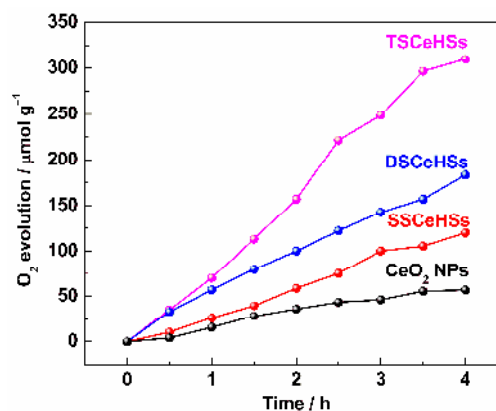

Fig. 3 O_2 evolution as a function of reaction time over commercial CeO_2 NPs, SSCeHSs, DSCeHSs and TSCeHSs in 0.01 M $AgNO_3$ aqueous solution under the UV-light irradiation (250 nm $<$ λ $<$ 380 nm).

The catalytic activity of TSCeHSs for photocatalytic water oxidation was further evaluated at various pH values and

different concentration of Ag^+ ions. Fig. S17 shows the O_2 evolution as a function of reaction time by photoirradiation at various pH values. When the initial pH value is decreased from 4.3 to 1.0, the O_2 evolution is dropped to 4% of its initial value,
5 suggesting that water oxidation preferably proceeds at higher pH value. This result is similar to previous report that the formed O_2 can capture conduction band electrons to form $O_2^{\bullet-}$ radical, and then reacts with H^+ ion in the low pH solution to produce $H_2O^{\bullet}$, causing a decrease in the O_2 evolution rate.[37] When the initial pH
10 value is further increased from 4.3 to 7.8, the O_2 evolution is dropped to 25% of its initial value. This may be attributed to the fact that Ag^+ ions can be hydrolyzed into precipitate by OH^- ions at high pH values, thus lowering the concentration of Ag^+ ions and decreasing the capture rate of photogenerated electrons. Fig.
15 S18 diplays the influence of Ag^+ ions on the O_2 evolution. When the concentration of $AgNO_3$ aqueous solution is decreased from 0.01 M to 0.0025 M, the O_2 evolution is dropped to 53% of its initial value. Meanwhile, when the concentration of $AgNO_3$ aqueous solution is increased from 0.01 M to 0.04 M, the O_2
20 evolution also dropped to 64% of its initial value. This could be understood that excessive Ag^+ ions are easily hydrolyzed to form the precipitate, which deposits on the surfaces of the TSCeHSs to cover the active sites, thus leading to a decrease in the O_2 evolution rate. The above results demonstrate that the maximized
25 O_2 evolution rate can be achieved by optimizing the pH value and the concentration of Ag^+ ions.

In addition to the activity, the stability is another key parameter to evaluate the performance of the catalysts. The stability of different samples was investigated by a series of repeated purge
30 and injection cycles with an interval of 4 h. It is seen from Table 1 and Fig. S19 that the order of the photocatalytic stability is as follows: TSCeHSs > DSCeHSs > SSCeHSs > commercial CeO_2 NPs. With increasing the cycle number, the photocatalytic stability shows a gradual decrease. The average O_2 evolution
35 rates are decreased from 14 $\mu mol\ g^{-1}_{cat}\ h^{-1}$ at the 1st cycle to 2 $\mu mol\ g^{-1}_{cat}\ h^{-1}$ at the 3rd cycle for the commercial CeO_2 NPs, from 30 $\mu mol\ g^{-1}_{cat}\ h^{-1}$ at the 1st cycle to 10 $\mu mol\ g^{-1}_{cat}\ h^{-1}$ at the 3rd cycle for the SSCeHSs, from 46 $\mu mol\ g^{-1}_{cat}\ h^{-1}$ at the 1st cycle to 20 $\mu mol\ g^{-1}_{cat}\ h^{-1}$ at the 3rd cycle for the DSCeHSs, and
40 from 78 $\mu mol\ g^{-1}_{cat}\ h^{-1}$ at the 1st cycle to 40 $\mu mol\ g^{-1}_{cat}\ h^{-1}$ at the

Table 1 Average O_2 evolution rate over four photocatalysts for direct water oxidation by a series of repeated purge and injection cycles with an interval of 4 h, and corresponding change of catalytic activity.

Samples	First cycle	Second cycle		Third cycle	
	O_2 evolution rate [a]	O_2 evolution rate [a]	Activity change [b] (%)	O_2 evolution rate [a]	Activity change [b] (%)
CeO_2 NPs	14	6	42.8	2	14.3
SSCeHSs	30	13	43.3	10	33.3
DSCeHSs	46	31	67.4	20	43.5
TSCeHSs	78	53	67.9	40	51.3

45 [a] The average O_2 evolution rate with the unit ($\mu mol\ g^{-1}_{cat}\ h^{-1}$) is calculated according to the data obtained from Fig. S19. [b] Activity of four photocatalysts after the second and third cycle accounts for the initial activity of the first cycle.

3rd cycle for the TSCeHSs, respectively. It is worth mentioning
50 that the TSCeHSs possess the best stability among all the samples, and the O_2 evolution rate dropped to 51.3% of the initial values after three cycles (Table 1).Why is the catalytic acivity decreased with the cycle number, and what is the reason for the TSCeHSs having the highest stability? To answer these
55 questions, four photocatalysts after three cycles of catalytic reactions are characterized. XRD pattern (Fig. S20) and elemental mapping by HAADF-STEM (Fig. S21) indicate that Ag^+ ions are reduced into Ag NPs by photogenerated electrons and some Ag NPs are deposited on the surface of the photocatalysts and block
60 the active sites, thus leading to a decrease in photocatalytic stability. Energy-dispersive X-ray spectroscopy (EDX) measurement further shows that the average content of the deposited Ag NPs in the TSCeHSs (2.2%) is much lower than that of the commercial CeO_2 NPs (10.9%), the SSCeHSs (5.4%)
65 and the DSCeHSs (4.9%). This finding highlights the unique advantages of the multi-shelled hollow microspheres as the water oxidation photocatalysts, that is, they have more curved surfaces that are unfavorable for nucleation and growth of Ag NPs. Therefore, Ag NPs prefer precipitating in soluton rather than
70 depositing on the surface of the TSCeHSs, giving rise to keeping exposure of the active sites and maintaining better catalytic stability.

In summary, a simple and facile "self-templating" approach was developed to construct the TSCeHSs by combination of
75 hydrothermal and calcination treatments. Impressively, with respect to the commercial CeO_2 NPs, the SSCeHSs and the DSCeHSs, the TSCeHSs exhibit the excellent activity and the improved stability for photocatalytic water oxidation with $AgNO_3$ as the electron scavenger. The outstanding catalytic performance
80 of the TSCeHSs is explored to be resulted from their unique properties: (1) Triple-shelled hollow structure allows for more multiple reflections of the incident light, and thus enhances the light-harvesting efficiency. (2) The larger surface area and the more active sites of the TSCeHSs are beneficial for separation of
85 the electron and hole pairs. (3) The more curved surfaces of the TSCeHSs make it more difficult for deposition of as-formed Ag NPs, resulting in the better stability. Notably, this "self-templating" approach is applicable for construction of many types of multi-shelled metal oxide hollow microspheres including
90 Fe_2O_3, CoO, NiO, CuO, ZnO, CdO and *etc.* (Fig. S22). More importantly, to our knowledge, this work presents the first report on applying the multi-shelled hollow structures as the photocatalysts for water decomposition reactions. Hence, we can expect that these multi-shelled hollow micor-/nano-structures
95 obtained with simple synthesis methods will offer many opportunities for new energy application.

Acknowledgements

Nanoscale Accepted Manuscript

Notes and references

ᵃ Laboratory for Nanomaterials, National Center for Nanoscience and Technology, Beijing 100190, P. R. China. Fax: (+86) 010-62656765. E-mail: zytang@nanoctr.cn

ᵇ Department of Physical Chemistry, University of Science and Technology Beijing, Beijing 100083, P. R. China. E-mail: ranboyu@ustb.edu.cn

ᶜ Centre for Clean Environment and Energy, Gold Cost Campus, Griffith University, Queensland 4222, Australia.

† Electronic Supplementary Information (ESI) available: [details of any supplementary information available should be included here]. See DOI: 10.1039/b000000x/

‡ These authors contributed equally to this work.

1　A. Fujishima and K. Honda, *Nature,* 1972, **238**, 37–38.

2　H. M. Chen, C. K. Chen, R. Liu, L. Zhang, J. Zhang and D. P. Wilkinsonc, *Chem. Soc. Rev.,* 2012, **41**, 5654–5671.

3　a) J. Duan, W. Shi, L. Xu, G. Mou, Q. Xin and J. Guan, *Chem. Commun.,* 2012, **48**, 7301–7303. b) N. Zhang, S. Liu and Y.-J. Xu, *Nanoscale,* 2012, **4**, 2227–2238. c) N. Zhang, Y. Zhang and Y.-J. Xu, *Nanoscale,* 2012, **4**, 5792–5813.

4　C. G. Silva, R. Juárez, T. Marino, R. Molinari and H. García, *J. Am. Chem. Soc.,* 2011, **133**, 595–602.

5　a) H. B. Wu, H. H. Hng and X. W.(David) Lou, *Adv. Mater.,* 2012, **24**, 2567–2571. b) X. Lu, T. Zhai, H. Cui, J. Shi, S. Xie, Y. Huang, C. Liang and Y. Tong, *J. Mater. Chem.,* 2011, **21**, 5569–5572.

6　H. Yan, *Chem. Commun.,* 2012, **48**, 3430–3432.

7　Y. Cong, J. Zhang, F. Chenand M. Anpo, *J. Phys. Chem. C,* 2007, **111**, 6976–6982.

8　a) X. Zong, H. Yan, G. Wu, G. Ma, F. Wen, L. Wang and C. Li, *J. Am. Chem. Soc.,* 2008, **130**, 7176–7177. b) M. Liu, L. Wang, G. (Max) Lu, X. Yao and L. Guo, *Energy Environ. Sci.,* 2011, **4**, 1372–1378. c) Y. Chen, L. Wang, G. (Max) Lu, X. Yao and L. Guo, *J. Mater. Chem.,* 2011, **21**, 5134–5141.

9　M. W. Kanan and D. G. Nocera, *Science,* 2008, **321**, 1072–1075.

10　a) C. G. Silva, Y. Bouizi, V. Fornés and H. García, *J. Am. Chem. Soc.,* 2009, **131**, 13833–13839. b) R. Liu, Y. Lin, L.-Y. Chou, S. W. Sheehan, W. He, F. Zhang, H. J. M. Hou and D. Wang, *Angew. Chem. Int. Ed.,* 2011, **50**, 499–502.

11　a) A. Primo, T. Marino, A. Corma, R. Molinari and H. García, *J. Am. Chem. Soc.,* 2011, **133**, 6930–6933. b) G. R. Bamwenda, T. Uesigi, Y. Abe, K. Sayama and H. Arakawa, *Appl. Catal. A- Gen.,* 2001, **205**, 117–128.

12　M. T. Mayer, Y. Lin, G. Yuan, D. Wang, *Acc. Chem. Res.,* 2013, **46**, 1558–1566.

13　a) W. J. Jo, J. -W. Jiang, K. -J. Kong, H. J. Kang, J. Y. Kim, H. Jun, K. P. S. Parmar and J. S. Lee, *Angew. Chem. Int. Ed.,* 2012, **51**, 3147–3151. b) D. Wang, H. Jiang, X. Zong, Q. Xu, Y. Ma, G. Li and C. Li, *Chem. Eur. J.,* 2011, **17**, 1275–1282. c) M. Zhou, H. B. Wu, J. Bao, L. Liang, X. W.(David) Lou and Y. Xie, *Angew. Chem. Int. Ed.,* 2013, **52**, 8679–8583.

14　S. J. Hong, S. Lee, J. S. Jang and J. S. Lee, *Energy Environ. Sci.,* 2011, **4**, 1781–1787.

15　a) M. Liao, J. Feng, W. Luo, Z. Wang, J. Zhang, Z. Li, T. Yu and Z. Zou, *Adv. Funct. Mater.,* 2012, **22**, 3066–3074. b) M.-R. Gao, Y.-F. Xu, J. Jiang, Y.-R. Zheng, S.-H. Yu, *J. Am. Chem. Soc.,* 2012, **134**, 2930–2933.

16　M. Ni, M. K. H. Leung, D. Y. C. Leung and K. Sumathy, *Renewable Sust. Energy Rev.,* 2007, **11**, 401–425.

17　D. Barreca, G. Carraro, V. Gombac, A. Gasparotto, C. Maccato, P. Fornasiero and E. Tondello, *Adv. Funct. Mater.,* 2011, **21**, 2611–2623.

18　Y. W. Chen, J. D. Prange, S. Düehnen, Y. Park, M. Gunji, C. E. Chidsey and P. C. Mcintyre, *Nat. Mater.,* 2011, **10**, 539–544.

19　X. Wu, G. Q. Lu and L. Wang, *Energy Environ. Sci.,* 2011, **4**, 3565–3572.

20　a) X. Lai, J. Li, B. A. Korgel, Z. Dong, Z. Li, F. Su, J. Du and D. Wang, *Angew. Chem. Int. Ed.,* 2011, **50**, 2738–2741. b) X. Wang, M. Liao, Y. Zhong, J. Y. Zheng, W. Tian, T. Zhai, C. Zhi, Y. Ma, J. Yao, Y. Bando and D. Golberg, *Adv. Mater.,* 2012, **24**, 3421–3425.

21　H. Xu and W. Wang, *Angew. Chem. Int. Ed.,* 2007, **46**, 1489–1492.

22　J. Wang, N. Yang, H. Tang, Z. Dong, Q. Jin, M. Yang, D. Kisailus, H. Zhao, Z. Tang and D. Wang, *Angew. Chem. Int. Ed.,* 2013, **52**, 6417–6420.

23　a) H. X. Yang, J. F. Qian, Z. X. Chen, X. P. Ai and Y. L. Cao, *J. Phys. Chem. C,* 2007, **111**, 14067–14071. b) X. W.(David) Lou, Y. Wang, C. Yuan, J. Y. Lee and L. A. Archer, *Adv. Mater.,* 2006, **18**, 2325–2329.

24　B. Wang, H. B. Wu, L. Zhang, X. W.(David) Lou, *Angew. Chem. Int. Ed.,* 2013, **52**, 4165–4168.

25　L. Wang, F. Tang, K. Ozawa, Z. -G. Chen, A. Mukherj, Y. Zhu, J. Zou, H. -M. Cheng and G. Q. (Max) Lu, *Angew. Chem. Int. Ed.,* 2009, **48**, 7048–7051.

26　a) Z. Wang, J. Hou, C. Yang, S. Jiao, K. Huang and H. Zhu, *Energy Environ. Sci.,* 2013, **6**, 2134–2144. b) L. Liu, W. Zou, X. Gu, C. Ge, Y. Deng, C. Tang, F. Gao, L. Dong and A. Corma, *J. Mater. Chem. A,* 2013, doi: 10.1039/C3TA13872K, in press.

27　a) Y. Lee, G. He, A. J. Akey, R. Si, M. Flytzani-Stephanopoulos and I. P. Herman, *J. Am. Chem. Soc.,* 2011, **133**, 12952–12955. b) J. Qi, J. Chen, G. Li, S. Li, Y. Gao and Z. Tang, *Energy Environ. Sci.,* 2012, **5**, 8937–8941. c) N. Zhang, X. Fu and Y.-J. Xu, *J. Mater. Chem.,* 2011, **21**, 8152–8158.

28　a) V. Salgueiriño-Maceira, M. Spasova and M. Farle, *Adv. Funct. Mater.,* 2005, **15**, 1036–1040. b) H. -P. Hentze, S. R. Raghavan, C. A. McKelvey and E. W. Kaler, *Langmuir,* 2003, **19**, 1069–1074. c) Y. Liu, J. Goebl and Y. Yin, *Chem. Soc. Rev.,* 2013, **42**, 2610–2653. d) J. B. Joo, M. Dahl, N. Li, F. Zaera and Y. Yin, *Energy Environ. Sci.,* 2013, **6**, 2082–2092. e) Q. Zhang, W. Wang, J. Goebl and Y. Yin, *Nano Today,* 2009, **4**, 494–507. f) H. B. Wu, A. Pan, H. H. Hng and X. W.(David) Lou, *Adv. Funct. Mater.,* 2013, **23**, 5669–5674. g) X. W.(David) Lou, L. A. Archer and Z. Yang, *Adv. Mater.,* 2008, **20**, 3987–40193.

29　M. Cargnello, C. Gentilini, T. Montini, E. Fonda, S. Mehraeen, M. Chi, M. Herrera-Collado, N. D. Browning, S. Polizzi, L. Pasquato and P. Fornasiero, *Chem. Mater.,* 2010, **22**, 4335–4345.

30　Z. Wu, D. Huang and X. Yang, *Vacuum,* 1998, **51**, 397–401.

31　X. Sun and Y. Li, *Angew. Chem. Int. Ed.,* 2004, **43**, 597–601.

32　W. Tian, L. -M. Yang, Y. -Z. Xu, S. -F. Weng and J. -G. Wu, *Carbohydr. Res.,* 2000, **324**, 45–52.

33　L. Han, R. Liu, C. Li, H. Li, C. Li, G. Zhang and J. Yao, *J. Mater. Chem.,* 2012, **22**, 17079–17085.

34　a) H. Li, Z. Bian, J. Zhu, D. Zhang, G. Li, Y. Huo, H. Li and Y. Lu, *J. Am. Chem. Soc.,* 2007, **129**, 8406–8407. b) J. Qian, P. Liu, Y. Xiao, Y. Jiang, Y. Cao, X. Ai and H. Yang, *Adv. Mater.,* 2009, **21**, 3663–3667.

35　a) W. J. Jo, J. -W. Jang, K.-j Kong, H. J. Kang, J. Y. Kim, H. Jun, K. P. S. Parmar and J. S. Lee, *Angew. Chem. Int. Ed.,* 2012, **51**, 3147–3151.b) L. Xi, P. D. Tran, S. Y. Chiam, P. S. Bassi, W. F. Mak, H. K. Mulmudi, S. K. Batabyal, J. Barber, J. S. C. Loo and L. H. Wong, *J. Phys. Chem. C,* 2012, **116**, 13884–13889.

36　A. Kudo and Y. Miseki, *Chem. Soc. Rev.,* 2009, **38**, 253–278.

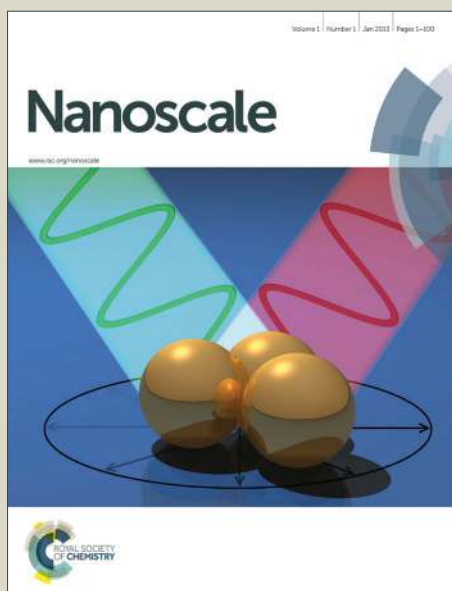37　M. A. Gondal, A. Hameed, Z. H. Yamani and A. Suwaiyan, *Appl. Catal. A-Gen.,* 2004, **268**, 159–167.
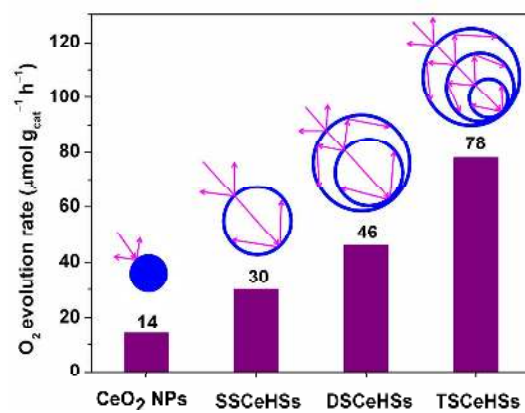
Nanoscale Accepted Manuscript

Table of content

A general self-templating method is introduced to construct triple-shelled CeO$_2$ hollow microspheres with the excellent photocatalytic activity for O$_2$ evolution.

This is an *Accepted Manuscript*, which has been through the Royal Society of Chemistry peer review process and has been accepted for publication.

Accepted Manuscripts are published online shortly after acceptance, before technical editing, formatting and proof reading. Using this free service, authors can make their results available to the community, in citable form, before we publish the edited article. We will replace this *Accepted Manuscript* with the edited and formatted *Advance Article* as soon as it is available.

You can find more information about *Accepted Manuscripts* in the **Information for Authors**.

Please note that technical editing may introduce minor changes to the text and/or graphics, which may alter content. The journal's standard **Terms & Conditions** and the **Ethical guidelines** still apply. In no event shall the Royal Society of Chemistry be held responsible for any errors or omissions in this *Accepted Manuscript* or any consequences arising from the use of any information it contains.